J Low Temp Phys (2014) 176:490–496
DOI 10.1007/s10909-014-1160-2

Dual-Polarization-Sensitive Kinetic Inductance Detectors for Balloon-borne Sub-millimeter Polarimetry

J. Hubmayr · J. A. Beall · D. Becker · J. A. Brevik · H. M. Cho · G. Che · M. Devlin · B. Dober · J. Gao · N. Galitzki · G. C. Hilton · K. D. Irwin · D. Li · P. Mauskopf · D. P. Pappas · J. Van Lanen · M. R. Vissers

Received: 15 July 2013 / Accepted: 4 March 2014 / Published online: 20 March 2014

Abstract We are developing arrays of kinetic inductance detectors for sub-millimeter polarimetry that will be deployed on the BLAST balloon-borne instrument. The array is feedhorn-coupled, and each pixel contains two lumped-element kinetic inductance detectors (LEKIDs) made of TiN. The absorbing, inductive sections of the LEKID-pair are orthogonal, which allows simultaneous measurement of both horizontal and vertical polarizations within one spatial pixel. In this paper, we show efficient absorption in TiN films when coupled to waveguide at room temperature and present dark measurements of single polarization devices with varying capacitor geometries. We show that it will be difficult to achieve background-limited performance in BLAST with stoichiometric TiN films with $T_c = 4.5$ K, and that non-stoichiometric films with lower T_c will be required.

Keywords KID · FIR · Detector · TiN · Polarimeter · Polarimetry

1 Introduction

Sub-millimeter (sub-mm) polarimetry enables interstellar magnetic field mapping, which is useful for studying dense star-forming regions [1]. The sensitivity achieved

J. Hubmayr (✉) · J. A. Beall · D. Becker · J. A. Brevik · H. M. Cho · J. Gao · G. C. Hilton · K. D. Irwin · D. Li · D. P. Pappas · J. Van Lanen · M. R. Vissers
National Institute of Standards and Technology, Boulder, CO, USA
e-mail: hubmayr@nist.gov

G. Che · P. Mauskopf
Arizona State University, Tempe, AZ, USA

M. Devlin · B. Dober · N. Galitzki
University of Pennsylvania, Philadelphia, PA, USA

with large-format arrays of low-temperature detectors has enabled such studies [2]. Li et al. [3] describe the advantages of a dual-beam polarimeter in the sub-mm, which simultaneously detects two orthogonal components of polarization. However, few detector technologies observing near 1 THz utilize dual-beam polarimetry. One notable example is the polarization sensitive bolometer used in Planck HFI [4].

We are developing arrays of dual-polarization-sensitive detectors that are based on kinetic inductance detectors (KIDs) [5]. A single spatial pixel is sensitive to both orthogonal components of linear polarization. A pixel contains two orthogonally crossed KIDs that are variations on the lumped-element kinetic inductance detector (LEKID) proposed and developed by Doyle [6]. The devices are fabricated from TiN, first demonstrated by Leduc [7] as a suitable material for superconducting devices. Benefits of TiN include high resistivity and kinetic inductance fraction, low observed loss and a tunable transition temperature [7,8].

In our design, the TiN LEKIDs act as absorbers of sub-mm radiation that lie behind feedhorns. Feedhorn-coupling provides a number of benefits. Feeds are polarization preserving and achieve well-defined illumination of the primary optics. They are an effective means of eliminating stray light absorption. The forward gain reduces the detector volume which, for the case of KIDs, increases the device sensitivity. Lastly, feeds allow increased pixel spacing. For a LEKID design, the extra space on the wafer can be filled with large interdigitated capacitors (IDCs), which have been shown to decrease noise attributed to two-level-systems [9,10].

These dual-polarization-sensitive detector arrays will be used in the BLAST instrument [11]. In this paper, we describe the current state of development after a brief overview of the plans for BLAST.

2 BLAST

BLAST is a balloon-borne, sub-mm imaging polarimeter, which is used to study the role of magnetic fields in star formation. The instrument has flown five times, twice as a polarimeter. We are currently building a new, cryogenic receiver for the payload that achieves 22-arcmin resolution, a 340 arcmin^2 field of view and a 32-fold increase in mapping speed as compared to the current BLAST instrument. Re-imaging optics produce a separate focal plane for each frequency band centered on 250, 350 and 500 μm. We will produce an array of feedhorn-coupled, polarization-sensitive KIDs for each frequency band. The array concept is shown in left panel of Fig. 1. The devices are front-side illuminated and couple to square waveguide. Table 1 details the number of pixels, expected loading and expected background NEP in each frequency band.

We plan to readout the arrays using 550 MHz bandwidth ROACH boards [12] and SiGe amplifiers [13]. Two ROACH boards and two amplifiers will be used for the 250 μm band array; one ROACH and amplifier will be used for each of the 350 and 500 μm bands.

3 Detector Design

The pixel design and simulated performance is detailed in [14]. We review the design briefly here. The right panel of Fig. 1 shows the 250 μm pixel schematic, which

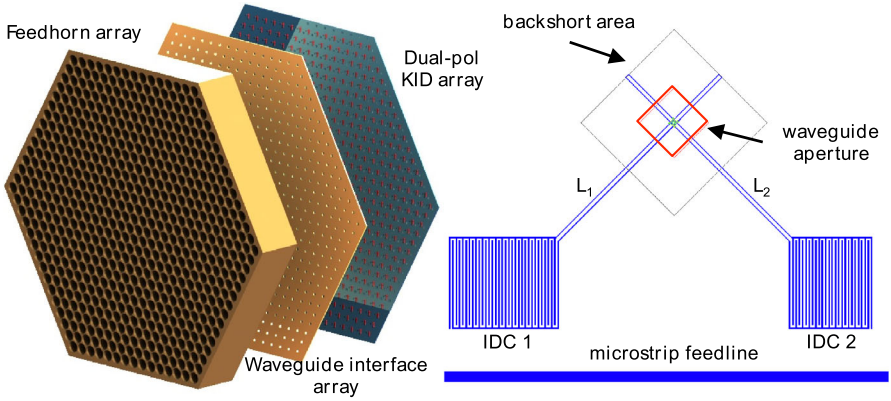

Fig. 1 *Left* Feedhorn-coupled array concept. *Right* dual-polarization-sensitive pixel design consisting of two orthogonally aligned TiN lumped-element kinetic inductance detectors (Color figure online)

Table 1 BLAST pixel count, photon power and predicted photon NEP

Center wavelengths (μm)	250	350	500
Number of detectors	1180	490	330
Background power (pW)	17	12	9
NEP_{photon} ($\times 10^{-17}$ W/$\sqrt{Hz}$)	17	12	8.7

consists of two lumped-element kinetic inductance detectors (LEKID), one for each polarization. The LEKIDs are made from TiN, deposited in the same deposition layer. The one-turn inductive section of a single LEKID serves as a single polarization absorber of sub-mm radiation, fed by square waveguide. The effective sheet impedance of the TiN inductive strips ($R_{s,eff} = R_{s,TiN} w/a$, where w and a are the width of the inductor strip and waveguide respectively) is matched to the waveguide impedance ($Z_{wg} = 377\Omega/\sqrt{1-(f_c/f)^2} \approx 700\ \Omega$, at 250 μm and $f_c = 1$ THz is the cut-off frequency of the waveguide). This impedance matching requirement constrains the volume of the active region of the KID. The inductors connect to ~0.6 mm^2 interdigitated capacitors (IDCs) that create resonant frequencies near 3 GHz. The LEKIDs are capacitively coupled to a cross-wafer microstrip feedline. The pixel spacing at 250 μm is 2.5 mm.

4 Optical Coupling

In this section, we describe a room temperature measurement that confirms our basic understanding of waveguide-coupled absorption in TiN structures. Our assumption is that the superconducting TiN sheet absorbs the same as a metal with the normal sheet impedance of TiN. Under this assumption, a room temperature absorption measurement should accurately reflect the absorption at cryogenic temperatures because the residual resistivity ratio (RRR) of TiN is near unity. To this end, we fabricate a TiN sample, which terminates the end of calibrated waveguide in a microwave vector network analyzer experimental setup. The reflection measurement off of the sample

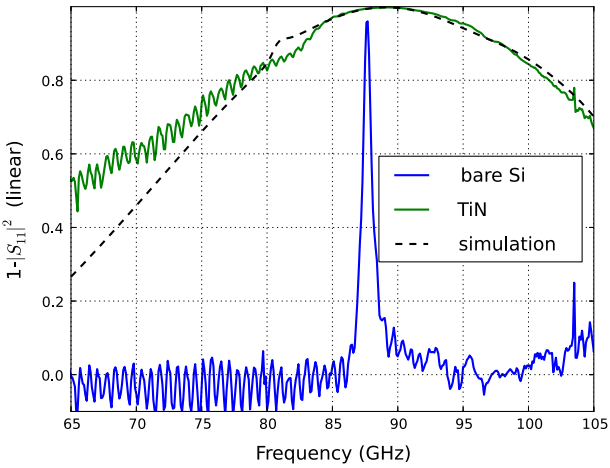

Fig. 2 Measurement of TiN absorption in WR10 waveguide at 300 K. Since $RRR \sim 1$, the measurement should be valid at cryogenic temperatures as well (Color figure online)

yields absorption because $S_{11}^2 < 1$ implies absorption. The 18 nm thick, 200 μm wide, one-turn TiN structure is fabricated on a 265 μm thick, >10 $k\Omega$·cm Si substrate. These absorber dimensions are not suitable for our detector design at 250 μm, but are scaled to W-band (65–110 GHz) in order to take advantage of existing measurement infrastructure. Here our goal is only to confirm our understanding of TiN absorption and validate our simulation models, not to explicitly predict the 250 μm band optical performance.

Figure 2 shows the measured absorption. The bare Si sample with no TiN does not absorb, except for the resonance at 87 GHz. The sample with the TiN structure, when aligned with the polarization direction of the waveguide, clearly exhibits absorption. The dashed, black line shows the predicted absorption for the TiN sample based on EM simulation assuming a sheet resistance $R_s = 130\ \Omega/\square$ and a relative dielectric constant in silicon of $\varepsilon_r = 11.9$. Agreement between measurement and simulation is very good, particularly above 80 GHz. We note that there is a 30 % higher sheet impedance implied from the simulation as compared to the measured DC value. The possibility of a frequency dependent sheet resistance requires further investigation. Nonetheless, this measurement demonstrates the efficacy of the optical coupling approach and the technique will aid in understanding the optical efficiency of future devices.

5 Single Polarization Test Devices

We fabricate single-polarization, single-layer test devices in effort to verify low loss, determine TiN material parameters and explore dark noise properties. We sputter-deposit a 17.5 nm thick TiN film on high-resistivity Si (>10 $k\Omega$·cm), and then pattern the film into the 12 LEKIDs shown in Fig. 3. The inductor volume is nearly constant for all resonators ($55 < V < 70\ \mu m^3$). There are four capacitor geometries, in which the IDC width and spacing are either 1, 2, 10 or 20 μm; however the total capacitance is the same for all geometries. The intent is to study noise attributed to a

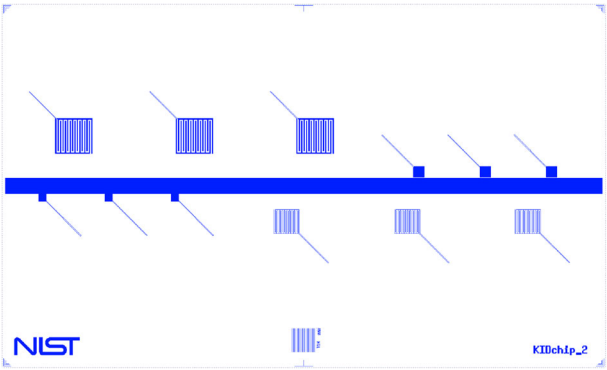

Fig. 3 Single polarization TiN LEKID chip design consisting of 12 resonators with four capacitor geometries (Color figure online)

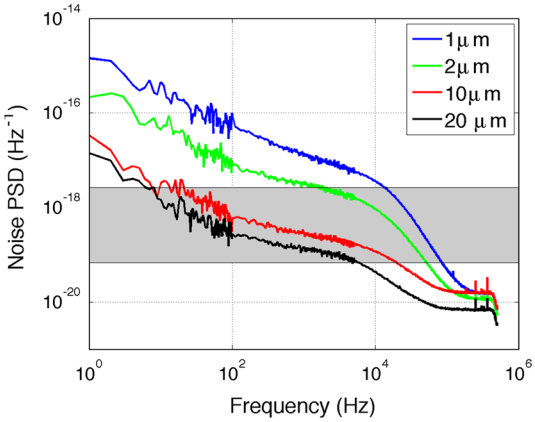

Fig. 4 PSD measured for each capacitor geometry at $T = 300$ mK and $P_g = -90$ dBm. The shaded region is a prediction of the photon noise level (Color figure online)

surface distribution of two-level system (TLS) fluctuators versus IDC geometry. We control the coupling quality factor, Q_c ~60,000, by the appropriate spacing to the 260 μm wide cross-wafer microstrip feed-line.

We measure $T_c = 4.4$ K, $\rho_n = 46$ μΩ·cm, $RRR = 1.08$ and determine the kinetic inductance fraction $\alpha = 0.95$. By use of standard homodyne readout with a ~4 K noise temperature HEMT amplifier, we measure the complex transmission S_{21} and fit the resonant circles to determine resonant frequencies ($2.55 < f_o < 2.8$ GHz) and quality factors. We find internal quality factors $1\times10^6 < Q_i < 3\times10^6$, consistent with other measurements of TiN loss [7,8].

The power spectral densities (PSDs) of the four capacitor geometries are presented in Fig. 4. We plot in units of fractional frequency shift, $x \equiv \delta f/f$, by use of the local slope $|dS_{21}/df|$ at the probe tone frequency. The noise is taken at $T = 300$ mK and $P_g \sim -90$ dBm, just below bifurcation [15]. Each spectrum shows three distinct regimes. The dominant noise source at low frequencies is attributed to TLS-induced frequency noise since we observe $S_x \sim f^{-0.5}$ [16]. Near 10 kHz the spectra roll off due to the resonator bandwidth. Above 100 kHz the spectra flatten to the white noise

level of the follow-on HEMT amplifier. The TLS fractional frequency noise decreases with increasing IDC gap and finger width w, scaling roughly as $S_{TLS} \sim w^{-1.2}$ when the noise is taken at 1 kHz.

The shaded region is a prediction for the single-polarization photon noise level:

$$S_{ph} = h\nu P_o(1+n_o)(\delta x/\delta P_o)^2 = h\nu P_o(1+n_o)(\frac{\alpha S_2 \eta_o \tau_{qp}}{4N_o\Delta^2 V})^2. \quad (1)$$

The form of the responsivity $(\delta x/\delta P_o)$ assumes the applicability of the Mattis–Bardeen equations [17]. The range of values for S_{ph} stem from incomplete knowledge of the single spin density of states N_o. The calculated value of $N_o = 8.7\times10^9$ eV$^{-1}\mu$m^{-3} [7], whereas the experimentally derived value for 1.4 K films is 3.9×10^{10} eV$^{-1}\mu$m^{-3} [18]. Additionally, there is a large uncertainty in the quasiparticle lifetime τ_{qp}, which we calculate assuming $\tau_{max} = 15$ µs [7] and $n^* = 100$ µm^3 [15]. The terms of the photon noise NEP are Planck's constant h, $\nu = 1.2$ THz, $P_o = 17$ pW and $n_o = 0.2$, the photon occupation number [19]. The responsivity $\delta x/\delta P_o$ includes the Mattis–Bardeen factor S_2 calculated assuming $T = 0.3$ K, $f = 2.7$ GHz and the superconducting gap $\Delta = 1.76k_b T_c = 0.67$ meV. $\eta_o = 0.7$ is the photon to quasiparticle conversion efficiency. $V = 60$ µm^3 is the detector volume.

6 Discussion and Conclusions

The measurements presented here show that TiN is an efficient absorber of mm-wave radiation, and we expect the same to hold at sub-mm wavelengths. Yet, our dark noise measurements indicate that the sensitivity of optically active pixels will be limited by TLS-noise if our knowledge of N_o and our estimation of τ_{qp} is correct. We intend to measure these quantities using single photon counting experiments following [18] as well as blackbody load-coupled noise measurements. Barring a surprising result, achieving background-limited performance on BLAST by use of stoichiometric TiN films will be challenging.

Sub-stoichiometric TiN resonators with $T_c < 4\ K$ and $f < 1$ GHz present an interesting parameter space, which we intend to investigate. The noise equivalent power of TLS-noise is expected to scale as T_c^4 [15]. Furthermore, as pointed out by several authors [15,20,21], frequency responsivity is enhanced at RF frequencies. With these scalings and using $T_c = 1.5$ K films, background-limited performance for BLAST should be attainable. Already, promising results of such TiN films have been demonstrated by researchers building the MAKO camera [20,21]. However, one complication of TiN films with $T_c < 4.5\ K$ is spatial non-uniformity, which is a major concern for detector array fabrication. Recently by use of Ti and TiN multi-layers, we show better than 1 % T_c variation across 75 mm diameter wafers for films with $0.8 < T_c < 2.5$ K [22]. Based on this result, the next step in our program is to test our LEKID design using these 1.4 K Ti/TiN multi-layer films.

Acknowledgments BLAST is funded by NASA through Grant No. NNX13AE50G S01. TiN materials research supported in part by DARPA. We thank the reviewers for thoughtful comments that improved the quality of this manuscript.

References

1. R.M. Crutcher, Astphys. Space Sci. **292**, 225 (2004)
2. A.D. Turner et al., Appl. Opt. **40**, 4921 (2001)
3. H. Li et al., Appl. Opt. **47**(3), 22 (2008)
4. W.C. Jones et al., Proc. of SPIE **4855**, 227 (2003)
5. P.K. Day et al., Nature **425**, 817 (2003)
6. S. Doyle et al., J. Low Temp. Phys. **151**, 530 (2008)
7. H.G. Leduc et al., Appl. Phys. Lett. **97**, 10 (2010)
8. M.R. Vissers et al., Appl. Phys. Lett. **97**, 23 (2010)
9. J. Gao et al., Appl. Phys. Lett. **92**, 212504 (2008)
10. O. Noroozian et al., AIP Conf. Ser. **1185**, 148 (2009)
11. E. Pascale et al., ApJ **681**, 400 (2008)
12. R. Duan et al., Proc of SPIE **7741**, 77411E (2010)
13. J.C. Bardin, Ph.D. dissertation, California Institute of Technology, Pasadena CA, 2009
14. Hubmayr et al., IEEE Trans. Appl. Sup. **23**, 2 (2012)
15. J. Zmuidzinas, Ann. Rev. of Cond. Mat. Phys. **3**, 1 (2012)
16. J. Gao et al., Appl. Phys. Lett. **92**, 152505 (2008)
17. D.C. Mattis, J. Bardeen, Phys. Rev. **111**, 412 (1958)
18. J. Gao et al., Appl. Phys. Lett. **101**, 142602 (2012)
19. J. Zmuidzinas, Appl. Opt. **42**, 4989 (2003)
20. L.J. Swenson et al., Proc. of SPIE **8452**, 84520P–1 (2012)
21. C.M. McKenney et al., Proc. of SPIE **8452**, 84520S–1 (2012)
22. M.R. Vissers et al., Appl. Phys. Lett. **102**, 232603 (2013)